

4

Experimental Methods

In earlier chapters we have discussed the results of a number of experiments, but said almost nothing about how such experiments are done. In this chapter we will take a brief look at experimental methods. This is a very extensive subject and the aim will not be to give a comprehensive review, but rather to emphasize the physical principles behind the methods. More details may be found in specialized texts.¹

4.1 Overview

To explore the structure of nuclei (nuclear physics) or hadrons (particle physics) requires projectiles whose wavelengths are at least as small as the effective radii of the nuclei or hadrons. This determines the minimum value of the momentum $p = h/\lambda$ and hence the energy required. The majority of experiments are conducted using beams of particles produced by machines called *accelerators*. This has the great advantage that the projectiles are of a single type, and have energies that may be controlled by the experimenter.² For example, beams that are essentially mono-energetic may be prepared, and can be used to study the energy dependence of interactions. The beam, once established, is directed onto a target so that interactions may be produced. In a *fixed-target* experiment the target is stationary in the laboratory. Nuclear physics experiments are almost invariably of this type, as are many experiments in particle physics.

In particle physics, high energies are also required to produce new and unstable particles and this reveals a disadvantage of fixed-target experiments when large

¹See, for example, Fe86 and K186.

²Nevertheless, important experiments are still performed without using accelerators, for example some of those described in Chapter 3 on neutrino oscillations used cosmic rays and nuclear reactors. In fact cosmic rays are still the source of the very highest-energy particles.

centre-of-mass energies are required. The centre-of-mass energy is important because it is a measure of the energy available to create new particles. In the laboratory frame at least some of the final-state particles must be in motion to conserve momentum. Consequently, at least some of the initial beam energy must reappear as kinetic energy of the final-state particles, and is therefore unavailable for particle production. In contrast, in the centre-of-mass frame the total momentum is zero and, in principle, all the energy is available for particle production.

To find the centre-of-mass energy we use the expression

$$E_{\text{CM}}^2 = (P_t + P_b)^2 c^2, \quad (4.1)$$

where P is the particle's four-momentum and the subscripts t and b refer to target and beam, respectively.³ For a fixed-target experiment in the laboratory we have

$$P_t = (m_t c, \mathbf{0}); \quad P_b = (E_L/c, \mathbf{p}_b). \quad (4.2)$$

Expanding Equation (4.1) gives

$$E_{\text{CM}}^2 = (P_t^2 + P_b^2 + 2P_t P_b) c^2 \quad (4.3)$$

and using $P_t^2 = m_t^2 c^2$ etc., together with the general result

$$P_i P_j = E_i E_j / c^2 - \mathbf{p}_i \cdot \mathbf{p}_j, \quad (4.4)$$

we have

$$E_{\text{CM}} = [m_b^2 c^4 + m_t^2 c^4 + 2m_t c^2 E_L]^{1/2}. \quad (4.5)$$

At high energies this increases only as $(E_L)^{1/2}$ and so an increasingly smaller fraction of the beam energy is available for particle production, most going to impart kinetic energy to the target.

In a *colliding-beam* accelerator, two beams of particles travelling in almost opposite directions are made to collide at a small or zero crossing angle. If for simplicity we assume the particles in the two beams have the same mass and laboratory energy E_L and collide at zero crossing angle, then the total centre-of-mass energy is

$$E_{\text{CM}} = 2E_L. \quad (4.6)$$

This increases linearly with the energy of the accelerated particles, and hence is a significant improvement on the fixed-target result. Colliding-beam experiments are not, however, without their own disadvantages. The colliding particles have to be stable, which limits the interactions that can be studied, and the collision rate in the intersection region is smaller than that achieved in fixed-target experiments, because the particle densities in the beams are low compared with a solid or liquid target.

³A brief summary of relativistic kinematics is given in Appendix B.

Finally, details of the particles produced in the collision (e.g. their momenta) are deduced by observing their interactions with the material of *detectors*, which are placed in the vicinity of the interaction region. A wide range of detectors is available. Some have a very specific characteristic, others serve more than one purpose. Modern experiments, particularly in particle physics, typically use several types in a single experiment.

In this chapter we start by describing some of the different types of accelerator that have been built, the beams that they can produce and also how beams of neutral and unstable particles can be prepared. Then we discuss the ways in which particles interact with matter, and finally review how these mechanisms are exploited in the construction of a range of particle detectors.

4.2 Accelerators and Beams

All accelerators use electromagnetic forces to boost the energy of stable charged particles. These are injected into the machine from a device that provides a high-intensity source of low-energy particles, for example an electron gun (a hot filament), or a proton ion source. The accelerators used for nuclear structure studies may be classified into those that develop a steady accelerating field (DC machines) and those in which radio frequency electric fields are used (AC machines). All accelerators for particle physics are of the latter type. We start with a brief description of DC machines.

4.2.1 DC accelerators

The earliest type of DC accelerator was the *Cockcroft–Walton machine*, in which ions pass through sets of aligned electrodes that are operated at successively higher potentials. These machines are limited to energies of about 1 MeV, but are still sometimes used as injectors as part of the multistage process of accelerating particles to higher energies.⁴

The most important DC machine in current use is the *van de Graaff accelerator* and an ingenious version of this, known as the *tandem van de Graaff*, that doubles the energy of the simple machine, is shown schematically in Figure 4.1. The key to this type of device is to establish a very high voltage. The van de Graaff accelerator achieves this by using the fact that the charge on a conductor resides on its outermost surface and hence if a conductor carrying charge touches another conductor it will transfer its charge to the outer surface of the second conductor.

⁴Sir John Cockcroft and Ernest Walton received the 1951 Nobel Prize in Physics for the development of their accelerator and the subsequent nuclear physics experiments they did using it.

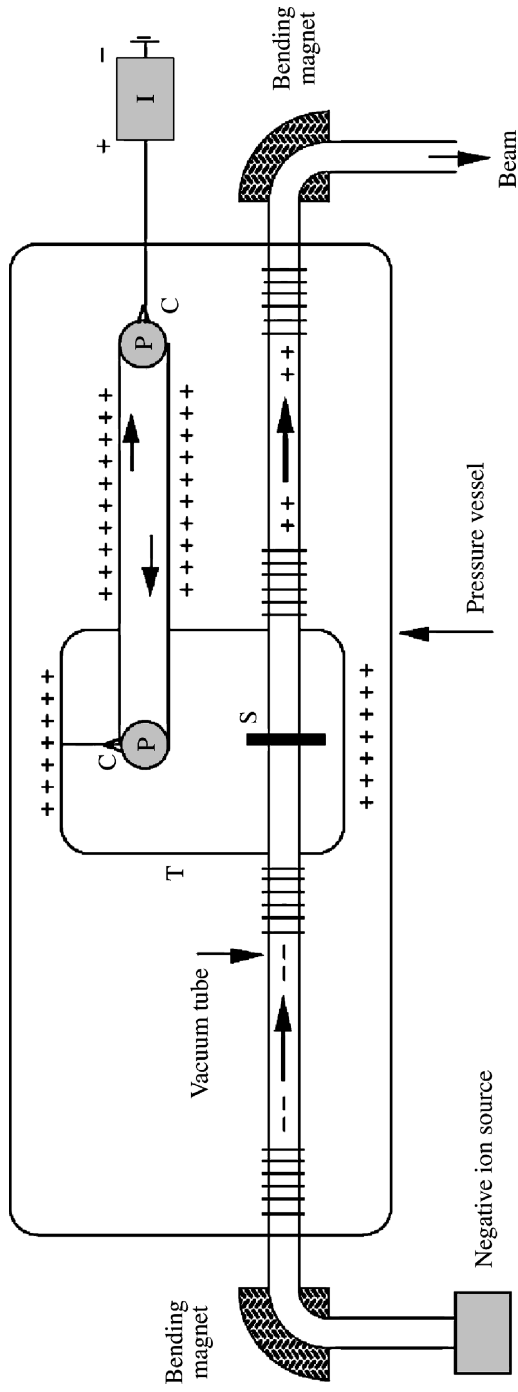


Figure 4.1 Principle of the tandem van de Graaff accelerator

In Figure 4.1, a high voltage source at I passes positive ions to a belt via a comb arrangement at C. The belt is motor driven via the pulleys at P and the ions are carried on the belt to a second pulley where they are collected by another comb located within a metal vessel T. The charges are then transferred to the outer surface of the vessel, which acts as an extended terminal. In this way a high voltage is established on T. Singly-charged negative ions are injected from a source and accelerated along a vacuum tube towards T. Within T there is a stripper S (for example a thin carbon foil) that removes two or more electrons from the projectiles to produce positive ions. The latter then continue to accelerate through the second half of the accelerator increasing their energy still further and finally may be bent and collimated to produce a beam of positive ions. This brief account ignores many technical details. For example, an inert gas at high pressure is used to minimize electrical breakdown by the high voltage. The highest energy van de Graaff accelerator can achieve a potential of about 30–40 MeV for singly-charged ions and greater if more than one electron is removed by the stripper. It has been a mainstay of nuclear research.

4.2.2 AC accelerators

Accelerators using radio frequency (r.f.) electric fields may conveniently be divided into *linear* and *cyclic* varieties.

Linear accelerators

In a linear accelerator (or *linac*) for accelerating ions, particles pass through a series of metal pipes called *drift tubes*, that are located in a vacuum vessel and connected successively to alternate terminals of an r.f. oscillator, as shown in Figure 4.2. Positive ions accelerated by the field move towards the first drift tube. If the

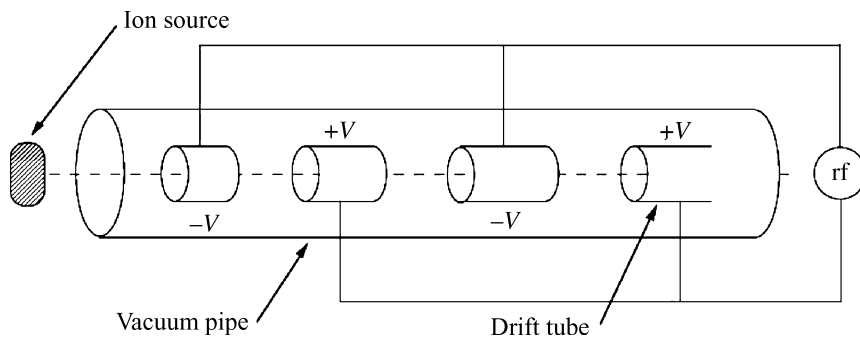


Figure 4.2 Acceleration in a linear ion accelerator

alternator can change its direction before the ions pass through that tube, then they will be accelerated again on their way between the exit of the first and entry to the second tube, and so on. Thus the particles will form bunches. Because the particles are accelerating, their speed is increasing and hence the lengths of the drift tubes have to increase to ensure continuous acceleration. To produce a useful beam the particles must keep in phase with the r.f. field and remain focused.

In the case of electrons, their velocity very rapidly approaches the speed of light. In this case a variation of the linac method that is more efficient is used to accelerate them. Bunches of particles pass through a straight evacuated waveguide with a periodic array of gaps, similar to the ion accelerator. Radio frequency oscillations in the gaps are used to establish a moving electromagnetic wave in the structure, with a longitudinal component of the electric field moving in phase with the particles. As long as this phase relationship can be maintained, the particles will be continuously accelerated. Radio frequency power is pumped into the waveguide at intervals to compensate for resistive losses and gives energy to the electrons. The largest electron linac is at the SLAC laboratory in Stanford, USA, and has a maximum energy of 50 GeV. It is over 3 km long.

An ingenious way of reducing the enormous lengths of high-energy linacs has been developed at the Continuous Electron Beam Accelerator Facility (CEBAF) at the Jefferson Laboratory in the USA. This utilizes the fact that above about 50 MeV, electron velocities are very close to the speed of light and thus electrons of very different energies can be accelerated in the same drift tube. Instead of a single long linac, the CEBAF machine consists of two much shorter linacs and the beam from one is bent and passed through the other. This can be repeated for up to four cycles. Even with the radiation losses inherent in bending the beams, very intense beams can be produced with energies between 0.5 and 6.0 GeV. CEBAF is proving to be an important machine in the energy region where nuclear physics and particle physics descriptions overlap.

Cyclic accelerators

Cyclic accelerators used for low-energy nuclear physics experiments are of a type called *cyclotrons*. They are also used to produce beams of particles for medical applications, including proton beams for radiation therapy. Cyclotrons operate in a somewhat different way to cyclic accelerators used in particle physics, which are called *synchrotrons*. In a cyclotron,⁵ charged particles are constrained to move in near-circular orbits by a magnetic field during the acceleration process. There are several types of cyclotron; we will describe just one. This is illustrated

⁵The cyclotron was invented by Ernest Lawrence, who received the 1939 Nobel Prize in Physics for this and the experimental work he did using it.

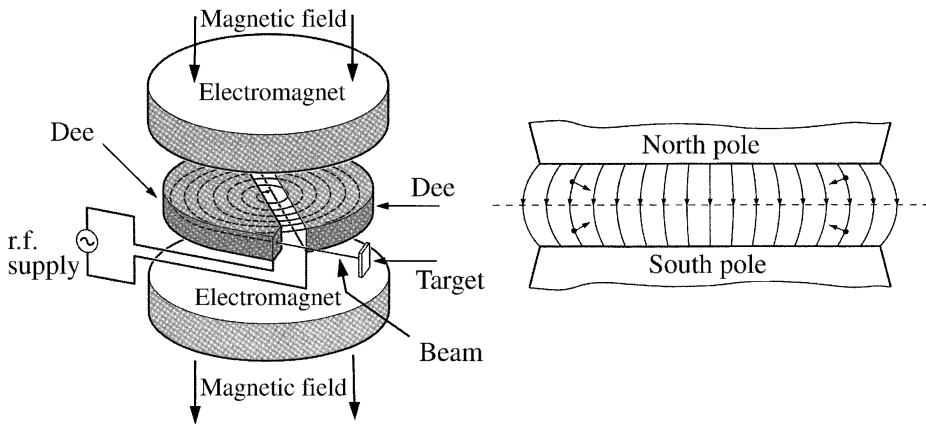


Figure 4.3 Schematic diagram of a cyclotron (adapted from Kr88, copyright John Wiley & Sons)

schematically in Figure 4.3. The accelerator consists of two ‘dee’-shaped sections across which an r.f. electric field is established. Charged ions are injected into the machine near its centre and are constrained to traverse outward in spiral trajectories by a magnetic field. The ions are accelerated each time they pass across the gap between the dees. At the maximum radius, which corresponds to the maximum energy, the beam is extracted. The shape of the magnetic field, which is also shown in Figure 4.3, ensures that forces act on particles not orbiting in the medium plane to move them closer to this plane. This brief description ignores the considerable problems that have to be overcome to ensure that the beam remains focused during the acceleration.

The principle of a *synchrotron* is analogous to that of a linear accelerator, but where the acceleration takes place in a near circular orbit rather than in a straight line. The beam of particles travels in an evacuated tube called the *beam pipe* and is constrained in a circular or near circular path by an array of dipole magnets called bending magnets (Figure 4.4). Acceleration is achieved as the beam repeatedly traverses one or more cavities placed in the ring where energy is given to the particles. Since the particles travel in a circular orbit they continuously emit radiation, called in this context *synchrotron radiation*. The amount of energy radiated per turn by a relativistic particle of mass m is proportional to $1/m^4$. For electrons the losses are thus very severe, and the need to compensate for these by the input of large amounts of r.f. power limits the energies of electron synchrotrons.

The momentum in GeV/c of an orbiting particle assumed to have unit charge is given by $p = 0.3B\rho$, where B is the magnetic field in Tesla and ρ , the radius of curvature, is measured in metres. Because p is increased during acceleration, B must also be steadily increased if ρ is to remain constant, and the final momentum is limited both by the maximum field available and by the size of the ring. With

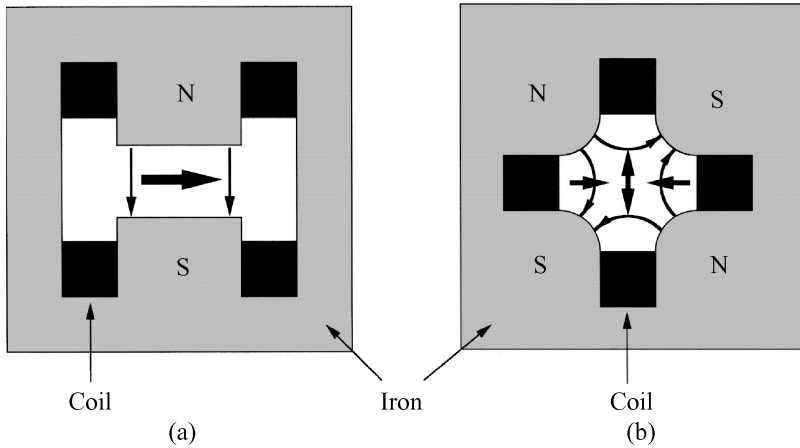


Figure 4.4 Cross-section of (a) a typical bending (dipole) magnet, and (b) a focusing (quadrupole) magnet; the thin arrows indicate field directions; the thick arrows indicate the force on a negative particle travelling into the paper

conventional electromagnets, the largest field attainable over an adequate region is about 1.5 T, and even with superconducting coils it is only of the order of 10 T. Hence the radius of the ring must be very large to achieve very high energies. For example, the Tevatron accelerator, located at the Fermi National Laboratory, Chicago, USA, which accelerates protons to an energy of 1 TeV, has a radius of 1 km. A large radius is also important to limit synchrotron radiation losses in electron machines.

In the course of its acceleration, a beam may make typically 10^5 traversals of its orbit before reaching its maximum energy. Consequently stability of the orbit is vital, both to ensure that the particles continue to be accelerated, and that they do not strike the sides of the vacuum tube. In practice, the particles are accelerated in bunches each being synchronized with the r.f. field. In equilibrium, a particle increases its momentum just enough to keep the radius of curvature constant as the field B is increased during one rotation, and the circulation frequency of the particle is in step with the r.f. of the field. This is illustrated in Figure 4.5. With obvious changes, a similar principle is used in linear accelerators.

In practice, the particles remain in the bunch, but their trajectories oscillate about the stable orbits. These oscillations are controlled by a series of focusing magnets, usually of the quadrupole type, which are placed at intervals around the beam and act like optical lenses. A schematic diagram of one of these is shown in Figure 4.4. Each focuses the beam in one direction and so alternate magnets have their field directions reversed.

In addition to the energy of the beam, one is also concerned to produce a beam of high intensity, so that interactions will be plentiful. The intensity is ultimately limited by defocussing effects, e.g. the mutual repulsion of the particles in the

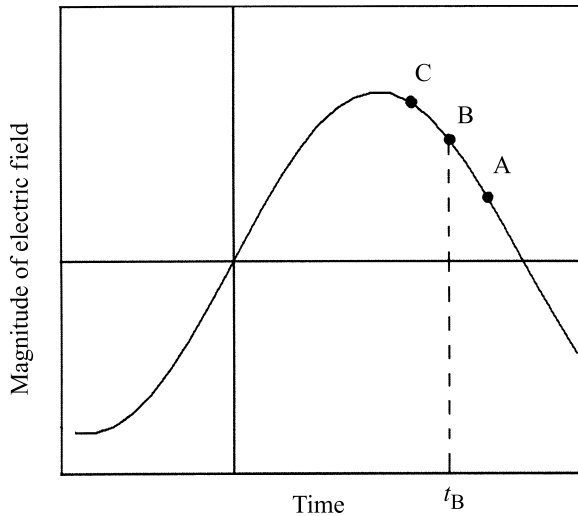


Figure 4.5 Magnitude of the electric field as a function of time at a fixed point in the rf cavity: particle B is synchronous with the field and arrives at time t_B ; particle A (C) is behind (ahead of) B and receives an increase (decrease) in its rotational frequency -- thus particles oscillate about the equilibrium orbit

beam, and a number of technical problems have to be overcome which are outside the scope of this brief account.⁶

Fixed-target machines and colliders

Both linear and cyclic accelerators can be divided into *fixed-target* and *colliding-beam* machines. The latter are also known as *colliders*, or sometimes in the case of cyclic machines, *storage rings*.⁷ In fixed-target machines, particles are accelerated to the highest operating energy and then the beam is extracted from the machine and directed onto a stationary target, which is usually a solid or liquid. Much higher energies have been achieved for protons than electrons, because of the large radiation losses inherent in electron machines mentioned earlier. The intensity of the beam is such that large numbers of interactions can be produced, which can either be studied in their own right or used to produce secondary beams.

The main disadvantage of fixed-target machines for particle physics has been mentioned earlier: the need to achieve large centre-of-mass energies to produce

⁶Very recently (2005) significant progress has been made on an 'induction synchrotron' in which a changing magnetic field produces the electric field that accelerates the particles. This device has the potential to overcome certain effects that limit the intensity achievable in conventional synchrotrons.

⁷The use of the terms *storage rings* and *colliders* as synonymous is not strictly correct, because we will see that the former can also describe a machine that stores a single beam for use on both internal and external fixed targets.

new particles. Almost all new machines for particle physics are therefore colliders, although some fixed-target machines for specialized purposes are still constructed. The largest collider currently under construction is the Large Hadron Collider (LHC), which is being built at CERN, Geneva, Switzerland. This is a massive pp accelerator of circumference 27 km, with each beam having an energy of 7 TeV. A schematic diagram of the CERN site showing the LHC and some of its other accelerators is shown in Figure 4.6. The acceleration process starts with a linac

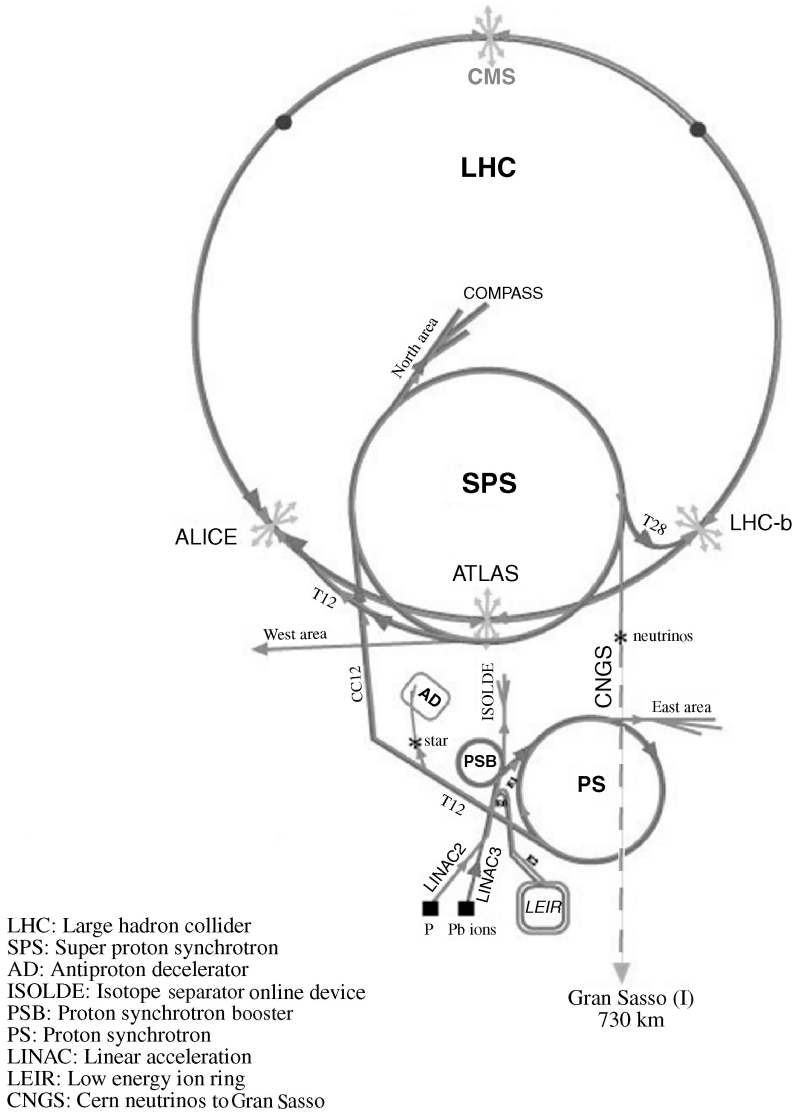


Figure 4.6 A schematic diagram of the CERN site showing the LHC and some of its other accelerators (CERN photo, reproduced with permission)

whose beam is boosted in energy in the Proton Synchrotron Booster (PSB) and passed to the Proton Synchrotron (PS), a machine that is still the source of beams for lower-energy experiments. The beam energy is increased still further in the Super Proton Synchrotron (SPS) that also provides beams for a range of experiments as well as the injection beams for the LHC itself. Four beam intersection points are shown in the LHC and experiments (ALICE, CMS, LHC-b and ATLAS) will be located at each of these. The extracted neutrino beam shown at the bottom of the diagram is sent to the Gran Sasso laboratory 730 km away and is used, amongst other things, for experiments on neutrino oscillations of the type discussed in Chapter 3.

Another very large collider we should mention is the Relativistic Heavy Ion Collider (RHIC), located at Brookhaven National Laboratory, USA. This unique machine, which began operation in 2000 following 10 years of development and construction, is the first collider in the world capable of accelerating heavy ions. Like the LHC above, there are several stages, involving a linac, a tandem van de Graaff and a synchrotron, before the ions are injected into the main machine. There they form two counter-circulating beams controlled by two 4-km rings of superconducting magnets and are accelerated to an energy of 100 GeV/nucleon. Thus the total centre-of-mass energy is 200 GeV/nucleon. Collisions occur at six intersection points, where major experiments can be sited. RHIC primarily accelerates ions of gold and is used to study matter at extreme energy-densities, where a new state of matter called a ‘quark–gluon plasma’ is predicted to occur. We will return to this briefly in Chapter 9.

The performance of a collider is characterized by its luminosity, which was defined in Chapter 1. The general formula for luminosity given there is shown in Problem 1.10 to reduce in the case of a collider to the useful form

$$L = n \frac{N_1 N_2}{A} f, \quad (4.7)$$

where $N_i (i = 1, 2)$ are the numbers of particles in the n colliding bunches, A is the cross-sectional area of the beam and f is the frequency, i.e. $f = 1/T$, where T is the time taken for the particles to make one traversal of the ring.

An interesting proton synchrotron for nuclear physics studies is the COSY facility located at the Research Centre Jülich, Germany. Low-energy protons are pre-accelerated in a cyclotron, then cooled to reduce their transverse momentum and injected into a synchrotron, where they are further accelerated to momenta in the range 600–3700 MeV/c (corresponding to energies of 175–2880 MeV). The protons can be stored in the ring for appreciable times and are available for experiments not only in the usual way by extracting the beam, but also by using the circulating beam to interact with a very thin internal target. Thus we have a mixture of storage rings and fixed targets. The fact that the circulating beam may make as many as 10^{10} traversals through the target compensates to some extent for its low particle density.

4.2.3 Neutral and unstable particle beams

The particles used in accelerators must be stable and charged, but one is also interested in the interaction of neutral particles, e.g. photons and neutrons, as well as those of unstable particles, such as charged pions. Beams appropriate for performing such experiments are produced in a number of ways.

We have seen that neutrons are the natural product of radioactive decays and we will see in Chapter 8 that a large flux of neutrons is present in a nuclear reactor. Typically these will have a spectrum concentrated at low energies of 1–2 MeV, but extending as high as 5–6 MeV. Purpose-built reactors exist for research purposes, such as the ILL reactor at the Institut Laue-Langevin, France. Another source of neutrons is via the spallation process. The most important neutron spallation source at present is ISIS located at the Rutherford Appleton Laboratory, UK. Protons which have been accelerated in a linac to 70 MeV are injected into a synchrotron that further accelerates them to 800 MeV, where they collide with a heavy metal target of tantalum. The interaction drives out neutrons from the target and provides an intense pulsed source. In each case, if beams of lower-energy neutrons are required these are produced by slowing down faster neutrons in moderators, which are materials with a large cross-section for elastic scattering, but a small cross-section for absorption. In Chapter 8 we will see that moderators are vital for the successful extraction of power from fission nuclear reactors.

Beams of unstable particles can be formed provided their constituents live long enough to travel appreciable distances in the laboratory. One way of doing this is to direct an extracted primary beam onto a heavy target. In the resulting interactions with the target nuclei, many new particles are produced which may then be analysed into secondary beams of well-defined momentum. Such beams will ideally consist predominantly of particles of one type, but if this cannot be achieved, then the wanted species may have to be identified by other means. In addition, if these secondary beams are composed of unstable particles, they can themselves be used to produce further beams formed from their decay products. Two examples will illustrate how, in principle, such secondary particle beams can be formed.

Consider firstly the construction of a K^- beam from a primary beam of protons. By allowing the protons to interact with a heavy target, secondary particles will be produced. Most of these will be pions, but a few will be kaons (that have to be produced with a hyperon to conserve strangeness – this an example of so-called *associated production*). A collimator can be used to select particles in a particular direction, and the K^- component can subsequently be removed and focused into a mono-energetic beam by selective use of electrostatic fields and bending and focusing magnets.

The pion beam may also be used to produce a beam of neutrinos. For example, the π^- is unstable and as we have seen, one of its weak interaction decays modes is $\pi^- \rightarrow \mu^- + \bar{\nu}_\mu$. So if the pions are passed down a long vacuum pipe, many will

decay in flight to give muons and anti-neutrinos, which will mostly travel in essentially the same direction as the initial beam. The muons and any remaining pions can then be removed by passing the beam through a very long absorber, leaving the neutrinos. In this case the final neutrino beam will have a momentum spectrum reflecting the initial momentum spectrum of the pions and, since neutrinos are neutral, no further momentum selection using magnets is possible.

4.3 Particle Interactions with Matter

In order to be detected, a particle must undergo an interaction with the material of a detector. In this section we discuss these interactions, but only in sufficient detail to be able to understand the detectors themselves.

The first possibility is that the particle interacts with an atomic nucleus. For example, this could be via the strong nuclear interaction if it is a hadron, or by the weak interaction if it is a neutrino. We know from the work of Chapter 1 that both are *short-range interactions*. If the energy is sufficiently high, new particles may be produced, and such reactions are often the first step in the detection process. In addition to these short-range interactions, a charged particle will also excite and ionize atoms along its path, giving rise to *ionization energy losses*, and emit radiation, leading to *radiation energy losses*. Both of these processes are due to the long-range electromagnetic interaction. They are important because they form the basis of most detectors for charged particles. Photons are also directly detected by electromagnetic interactions, and at high energies their interactions with matter lead predominantly to the production of e^+e^- pairs via the *pair production* process $\gamma \rightarrow e^+ + e^-$, which has to occur in the vicinity of a nucleus to conserve energy and momentum. (Recall the discussion in Chapter 1 on the range of forces.) All these types of interactions are described in the following sections.

4.3.1 Short-range interactions with nuclei

For hadrons, the most important short-range interactions with nuclei are due to the strong nuclear force which, unlike the electromagnetic interaction, is as important for neutral particles as for charged ones, because of the charge-independence of the strong interaction. Both elastic scattering and inelastic reactions may result. At high energies, many inelastic reactions are possible, most of them involving the production of several particles in the final state.

Many hadronic cross-sections show considerable structure at low energies due to the production of hadronic resonances, but at energies above about 3 GeV, total cross-sections are usually slowly varying in the range 10–50 mb and are much larger than the elastic cross-section. (The example of π^-p scattering is shown in Figure 4.7.) This is of the same order-of-magnitude as the ‘geometrical’

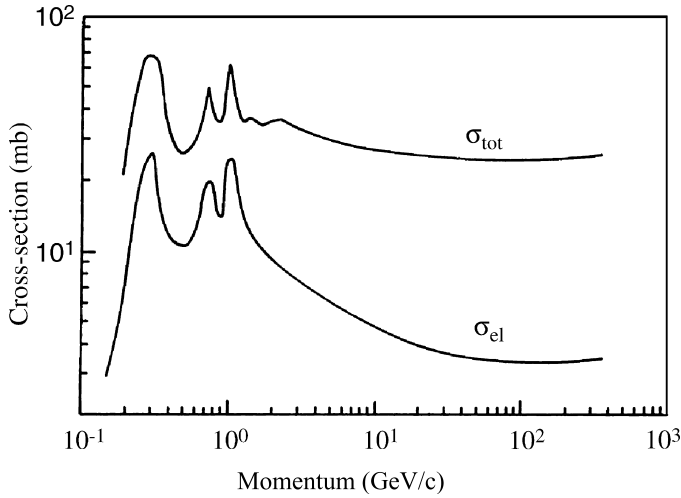


Figure 4.7 Total and elastic cross-sections for π^-p scattering as functions of the pion laboratory momentum

cross-section $\pi r^2 \approx 30$ mb, where $r \approx 1$ fm is the approximate range of the strong interaction between hadrons. Total cross-sections on nuclei are much larger see for example Figure (2.17), increasing roughly as the square of the nuclear radius, i.e. as $A^{2/3}$.

A special case is the detection of *thermal* neutrons (defined as those with kinetic energies below about 0.02 eV). We have seen in Chapter 2 that neutrons in this region have very large cross-sections for being absorbed, leading to the production of a compound nucleus which decays by delayed emission of a γ -ray. Examples of these so-called neutron activation reactions are $^{63}\text{Cu}(n, \gamma)^{64}\text{Cu}$ and $^{55}\text{Mn}(n, \gamma)^{56}\text{Mn}$.

The probability of a hadron-nucleus interaction occurring as the hadron traverses a small thickness dx of material is given by $n\sigma_{\text{tot}}dx$, where n is the number of nuclei per unit volume in the material. Consequently, the mean distance travelled before an interaction occurs is given by

$$\ell_c = 1/n\sigma_{\text{tot}}. \quad (4.8)$$

This is called the *collision length*. An analogous quantity is the *absorption length*, defined by

$$\ell_a = 1/n\sigma_{\text{inel}}, \quad (4.9)$$

that governs the probability of an inelastic collision. In practice, $\ell_c \approx \ell_a$ at high energies. As examples, the interaction lengths are between 10 and 40 cm for nucleons of energy in the range 100–300 GeV interacting with metals such as iron.

Neutrinos and antineutrinos can also be absorbed by nuclei, leading to reactions of the type

$$\bar{\nu}_\ell + p \rightarrow \ell^+ + X, \quad (4.10)$$

where ℓ is a lepton and X denotes any hadron or set of hadrons allowed by the conservation laws. Such processes are weak interactions (because they involve neutrinos) and the associated cross-sections are extremely small compared with the cross-sections for strong interaction processes. The corresponding interaction lengths are therefore enormous. Nonetheless, in the absence of other possibilities such reactions are the basis for detecting neutrinos. Finally, photons can be absorbed by nuclei, giving *photoproduction* reactions such as $\gamma + p \rightarrow X$. However, these electromagnetic interactions are only used to detect photons at low energies, because at higher energies there is a far larger probability for e^+e^- pair production in the Coulomb field of the nucleus. We will return to this in Section 4.3.4.

4.3.2 Ionization energy losses

Ionization energy losses are important for all charged particles, and for particles other than electrons and positrons they dominate over radiation energy losses at all but the highest attainable energies. The theory of such losses, which are due dominantly to Coulomb scattering from the atomic electrons, was worked out by Bethe, Bloch and others in the 1930s. The result is called the Bethe–Bloch formula, and for spin-0 bosons with charge $\pm q$ (in units of e), mass M and velocity v , it takes the approximate form (neglecting small corrections for highly relativistic particles)

$$-\frac{dE}{dx} = \frac{Dq^2n_e}{\beta^2} \left[\ln \left(\frac{2m_e c^2 \beta^2 \gamma^2}{I} \right) - \beta^2 \right], \quad (4.11)$$

where x is the distance travelled through the medium;

$$D = \frac{4\pi\alpha^2 \hbar^2}{m_e} = 5.1 \times 10^{-25} \text{MeV cm}^2, \quad (4.12)$$

m_e is the electron mass, $\beta = v/c$ and $\gamma = (1 - \beta^2)^{-1/2}$. The other constants refer to the properties of the medium: n_e is the electron density; I is the mean ionization potential of the atoms averaged over all electrons, which is given approximately by $I = 10Z \text{ eV}$ for Z greater than 20. The corresponding formula for spin- $\frac{1}{2}$ particles differs from this, but in practice the differences are small and may be neglected in discussing the main features of ionization energy losses.

Examples of the behaviour of $-dE/dx$ for muons, pions and protons traversing a range of materials is shown in Figure 4.8. It is common practice to absorb the density ρ of the medium by dividing by ρ and expressing dE/dx in terms of an

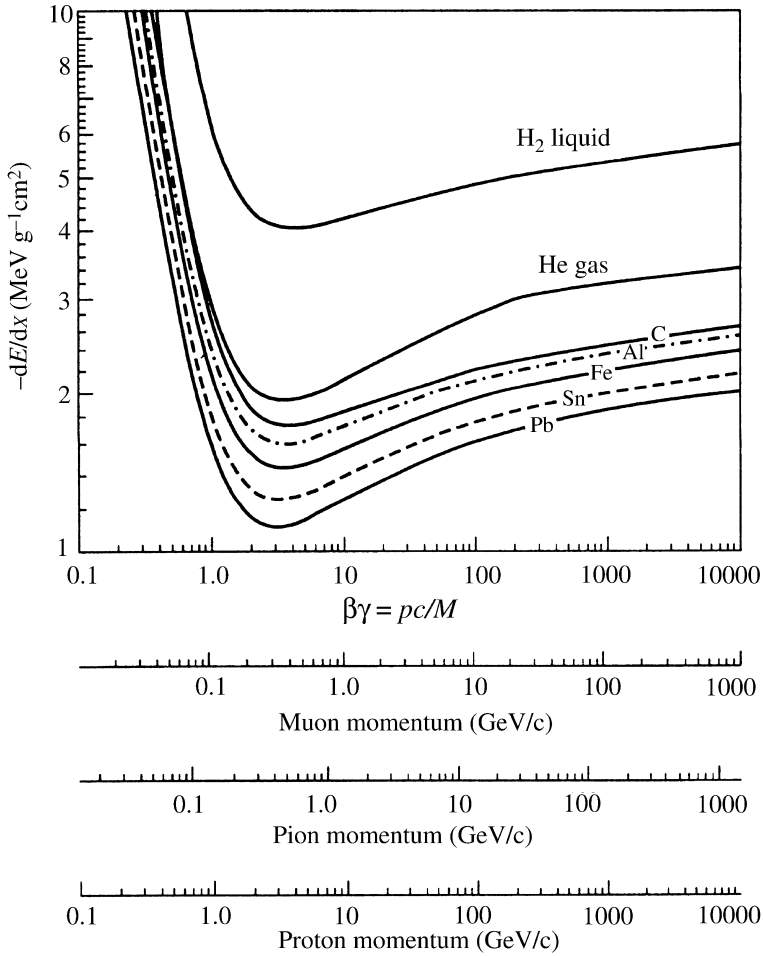


Figure 4.8 Ionization energy loss for muons, pions and protons on a variety of materials (reprinted from Ei04, copyright Elsevier, with permission)

equivalent thickness of gm cm^{-2} – hence the units in Figure 4.8. As can be seen, $-dE/dx$ falls rapidly as the velocity increases from zero because of the $1/\beta^2$ factor in the Bethe–Bloch equation. All particles have a region of ‘minimum ionization’ for $\beta\gamma$ in the range 3–4. Beyond this, β tends to unity, and the logarithmic factor in the Bethe–Bloch formula gives a ‘relativistic rise’ in $-dE/dx$.

The magnitude of the energy loss depends on the medium. The electron density is given by $n_e = \rho N_A Z/A$, where N_A is Avogadro’s number, and ρ and A are the mass density and atomic weight of the medium, so the mean energy loss is proportional to the density of the medium. The remaining dependence on the medium is relatively weak because $Z/A \approx 0.5$ for all atoms except the very light

and the very heavy elements, and because the ionization energy I only enters the Bethe–Bloch formula logarithmically. In the ‘minimum ionization’ region where $\beta\gamma \approx 3\text{--}4$, the minimum value of $-dE/dx$ can be calculated from Equation (4.11) and for a particle with unit charge is given approximately by

$$\left(-\frac{dE}{dx}\right)_{\min} \approx 3.5 \frac{Z}{A} \text{MeVg}^{-1} \text{cm}^2. \quad (4.13)$$

Ionization losses are proportional to the squared charge of the particle, so that a fractionally charged particle with $\beta\gamma \geq 3$ would have a much lower rate of energy loss than the minimum energy loss of any integrally charged particle. This has been used as a means of identifying possible free quarks, but without success.

From the knowledge of the rate of energy loss, we can calculate the attenuation as a function of distance travelled in the medium. This is called the *Bragg curve*. Most of the ionization loss occurs near the end of the path where the speed is smallest and the curve has a pronounced peak (the *Bragg peak*) close to the end point before falling rapidly to zero at the end of the particle’s path length. The *range* R , i.e. the mean distance a particle travels before it comes to rest is defined as

$$R \equiv \int_0^{x_{\max}} dx(\beta), \quad (4.14)$$

which, using Equation (4.11), may be written

$$R = \int_0^{\beta_{\text{initial}}} \left[-\frac{dE}{dx}\right]^{-1} \frac{dE}{d\beta} d\beta = \frac{M}{q^2 n_e} F(\beta_{\text{initial}}), \quad (4.15)$$

where F is a function of the initial velocity and we have used the relation $E = \gamma Mc^2$ to show the dependence on the projectile mass M .

The range as given by Equation (4.15) is actually an average value because scattering is a statistical process and there will therefore be a spread of values for individual particles. The spread will be greater for light particles and smaller for heavier particles such as α -particles. These properties have implications for the use of radiation in therapeutic situations, where it may be necessary to deposit energy within a small region at a specific depth of tissue, for example to precisely target a cancer. The biological effects of radiation will be discussed in Chapter 8.

Because neutrons are uncharged, direct detection is not possible by ionization methods. However, they can be detected via the action of the charged products of induced direct nuclear reactions. Commonly used reactions are ${}^6\text{Li}(n, \alpha){}^3\text{H}$, ${}^{10}\text{B}(n, \alpha){}^7\text{Li}$ and ${}^3\text{He}(n, p){}^3\text{H}$. All these reactions are exothermic and so are very suitable for detecting neutrons with energies below about 20 MeV. Moreover, as nuclear cross-sections tend to increase as v^{-1} at low energies, detection becomes more efficient the slower the neutron.

4.3.3 Radiation energy losses

When a charged particle traverses matter it can also lose energy by radiative collisions, especially with nuclei. The electric field of a nucleus will accelerate and decelerate the particles as they pass, causing them to radiate photons, and hence lose energy. This process is called *bremstrahlung* (literally ‘braking radiation’ in German) and is a particularly important contribution to the energy loss for electrons and positrons.

The dominant Feynman diagrams for electron bremsstrahlung in the field of a nucleus, i.e.

$$e^- + (Z, A) \rightarrow e^- + \gamma + (Z, A), \quad (4.16)$$

are shown in Figure 4.9 and are of the order of $Z^2\alpha^3$. The function of the nucleus is to absorb the recoil energy and so ensure that energy and momentum are simultaneously conserved (recall the discussion of Feynman diagrams in Chapter 1).

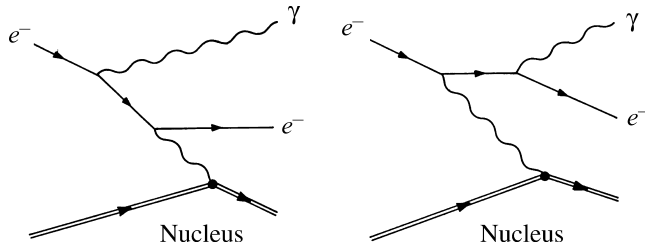


Figure 4.9 Dominant Feynman diagrams for the bremsstrahlung process $e^- + (Z, A) \rightarrow e^- + \gamma + (Z, A)$

There are also contributions from bremsstrahlung in the fields of the atomic electrons, each of the order of α^3 . Since there are Z atomic electrons for each nucleus, these give a total contribution of the order of $Z\alpha^3$, which is small compared with the contribution from the nucleus for all but the lightest elements. A detailed calculation shows that for relativistic electrons with $E \gg mc^2/\alpha Z^{1/3}$, the average rate of energy loss is given by

$$-dE/dx = E/L_R. \quad (4.17)$$

The constant L_R is called the *radiation length* and is a function of Z and n_a , the number density of atoms/cm³ in the medium. Integrating Equation (4.17) gives

$$E = -E_0 \exp(-x/L_R), \quad (4.18)$$

where E_0 is the initial energy. It follows that the radiation length is the average thickness of material that reduces the mean energy of an electron or positron by a factor e . For example, the radiation length in lead is 0.566 cm.

From these results, we see that at high energies the radiation losses are proportional to E/m_p^2 for an arbitrary charged particle of mass m_p . On the other

hand, the ionization energy losses are only weakly dependent on the projectile mass and energy at very high energies. Consequently, radiation losses completely dominate the energy losses for electrons and positrons at high enough energies, but are much smaller than ionization losses for all particles other than electrons and positrons at all but the highest energies.

Taking into account the above and the results of Section 4.3.2, we see that at low energies, particles with the same kinetic energy but different masses can have substantially different ranges. Thus, for example, an electron of 5 MeV has a range that is several hundred times that of an α -particle of the same kinetic energy.

4.3.4 Interactions of photons in matter

In contrast to heavy charged particles, photons have a high probability of being absorbed or scattered through large angles by the atoms in matter. Consequently, a collimated monoenergetic beam of I photons per second traversing a thickness dx of matter will lose

$$dI = -I \frac{dx}{\lambda} \quad (4.19)$$

photons per second, where

$$\lambda = (n_a \sigma_\gamma)^{-1} \quad (4.20)$$

is the mean free path before absorption or scattering out of the beam, and σ_γ is the total photon interaction cross-section with an atom. The mean free path λ is analogous to the collision length for hadronic reactions. Integrating Equation (4.19) gives

$$I(x) = I_0 e^{-x/\lambda} \quad (4.21)$$

for the intensity of the beam as a function of distance, where I_0 is the initial intensity.

The main processes contributing to σ_γ are: *Rayleigh scattering*, in which the photon scatters coherently from the atom, the *photoelectric effect*, in which the photon is absorbed by the atom as a whole with the emission of an electron; *Compton scattering*,⁸ where the photon scatters from an atomic electron; and *electron-positron pair production* in the field of a nucleus or of an atomic electron. The corresponding cross-sections on carbon and lead are shown in Figure 4.10, where it can be seen that above a few MeV the cross-section is dominated by pair production from the nucleus. The pair production process is closely related to

⁸Arthur Compton shared the 1927 Nobel Prize in Physics for the discovery of the increase in wavelength that occurs when photons with energies of around 0.5–3.5 MeV interact with electrons in a material – the original *Compton effect*.

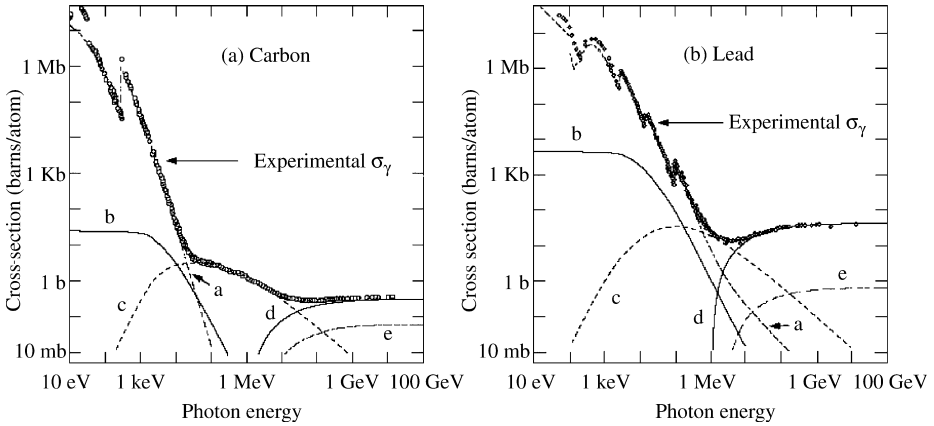


Figure 4.10 Total experimental photon cross-section σ_γ on (a) a carbon atom, and (b) a lead atom, together with the contributions from (a) the photoelectric effect, (b) Rayleigh (coherent atomic) scattering, (c) Compton scattering, (d) pair production in the field of the nucleus, and (e) pair production in the field of the atomic electrons (adapted from Ei04, copyright Elsevier, with permission)

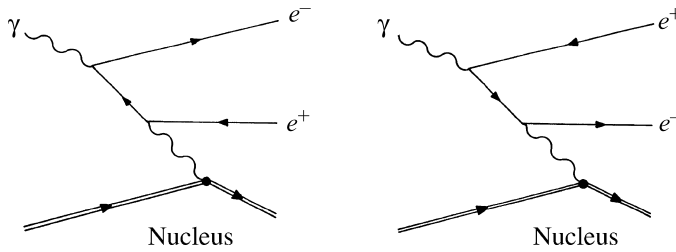


Figure 4.11 The pair production process $\gamma + (Z, A) \rightarrow e^- + e^+ + (Z, A)$

electron bremsstrahlung, as can be seen by comparing the Feynman diagrams shown in Figures 4.9 and 4.11.

The cross-section for pair production rises rapidly from threshold, and is given to a good approximation by

$$\sigma_{\text{pair}} = \frac{7}{9} \frac{1}{n_a L_R}, \quad (4.22)$$

for $E_\gamma \gg mc^2/\alpha Z^{1/3}$, where L_R is the radiation length. Substituting these results into Equation (4.21), gives

$$I(x) = I_0 \exp(-7x/9L_R), \quad (4.23)$$

so that at high energies, photon absorption, like electron radiation loss, is characterized by the radiation length L_R .

4.4 Particle Detectors

The detection of a particle means more than simply its localization. To be useful this must be done with a resolution sufficient to enable particles to be separated in both space and time in order to determine which are associated with a particular event. We also need to be able to identify each particle and measure its energy and momentum. No single detector is optimal with respect to all these requirements, although some are multifunctional. For example, calorimeters, primarily used for making energy measurements, can also have very good space and time resolution. Many of the devices discussed below are commonly used both in nuclear and particle physics, but in the former a small number of types of detector is often sufficient, whereas in particle physics, both at fixed-target machines and colliders, modern experiments commonly use very large multi-component detectors which integrate many different sub-detectors in a single device. Such systems rely heavily on fast electronics and computers to monitor and control the sub-detectors, and to coordinate, classify and record the vast amount of information flowing in from different parts of the apparatus. In this section we will briefly introduce some of the most important detectors currently available, but detector development is a rapidly-moving major area of research and new devices are frequently developed, so the list below is by no means exhaustive.⁹

4.4.1 Gas detectors

Most gas detectors detect the ionization produced by the passage of a charged particle through a gas, typically an inert one such as argon, either by collecting the ionization products or induced charges onto electrodes, or (historically) by making the ionization track visible in some form. The average energy needed to produce an electron-ion pair is 30 ± 10 eV, with a weak dependence on the gas used and the energy of the incident particle. In practice, the output is a pulse at the anode (which is amplified by electronic means), with the bulk of the signal being due to the positive ions because of their longer drift distance. For a certain range of applied voltages – the so-called ‘proportional region’ (see below) – these devices are primarily used to provide accurate measurements of a particle’s position. As position detectors, gas detectors largely replaced earlier detectors which used visual techniques, such as cloud chambers, bubble chambers and stacks of photographic emulsions, although the latter are still an ingredient in some neutrino experiments. Although historically important, none of these visual devices are now

⁹For more detailed discussions of particle detectors see, for example, Gr96 and the references in Footnote 1. There are also useful reviews in Chapter 5 of Ho97 and Ei04.

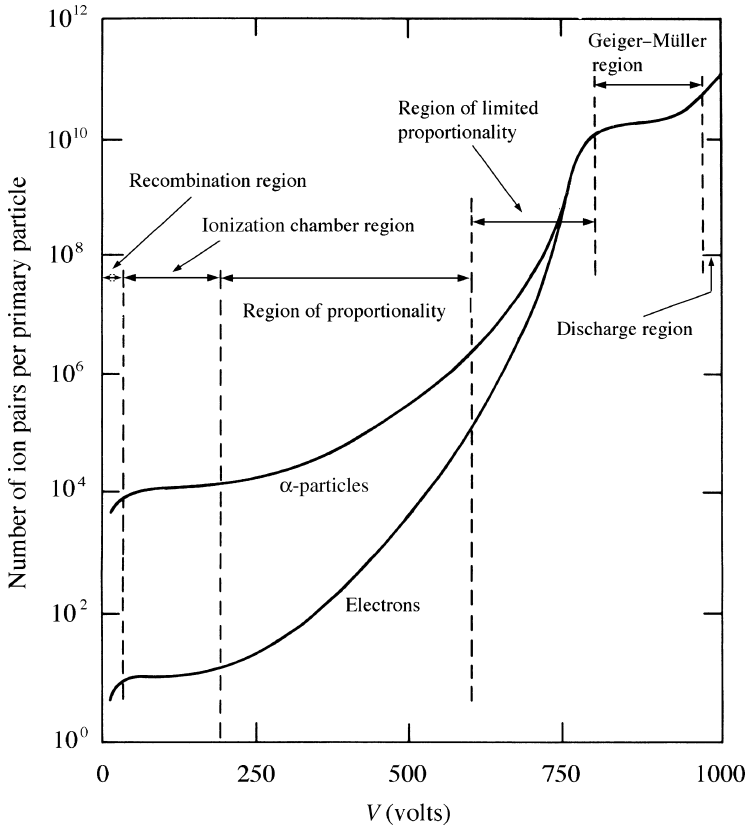


Figure 4.12 Gas amplification factor as a function of voltage V applied in a single-wire gas detector, with a wire radius typically $20\ \mu\text{m}$, for a strongly ionizing particle (α) and a weakly ionizing particle (electron)

in general use and they have been superseded by electronic detectors.¹⁰ In particle physics experiments being planned at the new accelerators currently being built, gas detectors themselves are being replaced by a new generation of solid-state detectors based on silicon.

To understand the principles of gas detectors we refer to Figure 4.12, which shows the number of ion pairs produced per incident charged particle (the *gas*

¹⁰These early detector techniques produced many notable discoveries and their importance has been recognized by the award of no less than five Nobel Prizes in Physics: a share of the 1927 Prize to Charles Wilson for the invention and use of the cloud chamber; the 1948 Prize to Patrick Blackett for further developments of the cloud chamber and discoveries made with it; the 1950 Prize to Cecil Powell for development of the photographic emulsion technique and its use to discover pions; the 1960 Prize to Donald Glaser for the invention of the bubble chamber; and the 1968 Prize to Luis Alvarez for developing the bubble chamber and associated data analysis techniques resulting in the discovery of a large number of hadronic resonances.

amplification factor) as a function of the applied voltage V for two cases: a heavily ionizing particle (e.g. an alpha particle – upper curve) and a lightly ionizing particle (e.g. an electron – lower curve).

Ionization chamber

At low applied voltages, the output signal is very small because electron–ion pairs recombine before reaching the electrodes, but as the voltage increases the number of pairs increases to a saturation level representing complete collection. This is the region of the *ionization chamber*. The simplest type of chamber is a parallel plate condenser filled with an inert gas and having an electric field $E = V/d$, where d is the distance between the plates. In practice the gas mixture must contain at least one ‘quenching’ component that absorbs ultraviolet light and stops a plasma forming and spreading throughout the gas.

Another arrangement is cylindrical with an inner anode of radius r_a and an outer cathode of radius r_c , giving an electric field

$$E(r) = \frac{V}{r \ln(r_c/r_a)} \quad (4.24)$$

at a radial distance r from the centre of the anode wire. The output signal is proportional to the number of ions formed and hence the energy deposited by the radiation, but is independent of the applied voltage. However, the signal is very small compared with the noise of all but the slowest electronic circuits and requires considerable amplification to be useful. Overall, the energy resolution and the time resolution of the chamber are relatively poor and ionization chambers are of very limited use in recording individual pulses. They are used, for example, as beam monitors, where the particle flux is very large, and in medical environments to calibrate radioactive sources.

As mentioned previously, neutrons cannot be directly detected by ionization methods, but neutron flux measurements can be made with ionization chambers (or proportional chambers – see below) filled with BF_3 by utilizing the neutron activation reactions of Section 4.3.1.

Proportional counters

If the voltage is increase beyond the region of operation of the ionization chamber, we move into the *proportional region*. In this region, a cylindrical arrangement as used in the ionization chamber will produce electric field strengths of the order of 10^4 – 10^5 V/cm near the wire and this is strong enough for electron–ion pairs released in the primary ionization to gain sufficient energy to cause secondary ionization. The rapid increase in amplification due to secondary ionization is called a *Townsend avalanche*. The output signal at the anode is still proportional to the

energy lost by the original particle. There are a number of different types of device working in the proportional region and they are sometimes generically referred to as *track chambers* or *wire chambers*.

The earliest detector using this idea was the *proportional counter*, which consists of a cylindrical tube filled with gas (again a quenching component in the gas is required) and maintained at a negative potential, and a fine central anode wire at a positive potential. Again, neutrons can be detected indirectly by using the direct nuclear reaction ${}^3\text{He}(n, p){}^3\text{H}$ mentioned in Section 4.3.2 in a proportional chamber filled with a mixture of ${}^3\text{He}$ and krypton. Subsequently, the resolution of proportional counters was greatly improved as a result of the discovery that if many anode wires were arranged in a plane between a common pair of cathode plates, each wire acts as an independent detector. This device is called a *multiwire proportional chamber* (MWPC), and was introduced in 1968.¹¹ An MWPC can achieve spatial resolutions of 200 μm or less, and has a typical time resolution of about 3 ns.

A schematic diagram of an MWPC is shown in Figure 4.13. The planes (a) have anode wires into the page and those in plane (b) are at right angles. The wire spacings are typically 2 mm. The cathodes are the faces of the chambers. A positive voltage applied to the anode wires generates a field as shown in the upper corner. A particle crossing the chamber ionizes the gas and the electrons drift along the field lines to the anode wires. In this particular example, there would be signals from one wire in the upper (a) chamber and two in the lower (a) chamber.

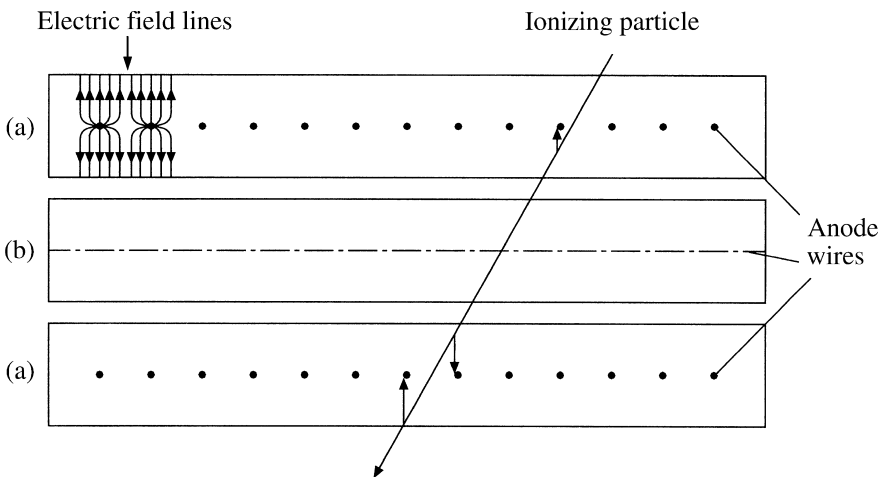


Figure 4.13 A group of three planes of an MWPC (from Po00 with kind permission of Springer Science and Business Media)

¹¹The MWPC was invented by Georges Charpak and for this and other developments in particle detectors he was awarded the 1992 Nobel Prize in Physics.

Even better spatial resolutions are obtained in a related device called a *drift chamber*, which has now largely replaced the MWPC as a general detector.¹² This uses the fact that the liberated electrons take time to drift from their point of production to the anode. Thus the time delay between the passage of a charged particle through the chamber and the creation of a pulse at the anode is related to the distance between the particle trajectory and the anode wire. In practice, additional wires are incorporated to provide a relatively constant electric field in each cell in a direction transverse to normal incidence. A reference time has to be defined, which, for example, could be done by allowing the particle to pass through a scintillator positioned elsewhere in the experiment (scintillation counters are discussed in Section 4.4.2). The electrons drift for a time and are then collected at the anode, thus providing a signal that the particle has passed. If the drift time can be measured accurately (to within a few ns) and if the drift velocity is known, then spatial resolutions of 100–200 μm can easily be achieved, and specialized detectors can reduce this still further.

Drift chambers are constructed in a variety of geometries to suit the nature of the experiment, and arrangements where the wires are in planar, radial or cylindrical configurations have all been used. The latter type is also called a ‘jet chamber’ and a two-jet event in a jet chamber was shown in Figure 3.5 as evidence for the existence of quarks.

One of the most advanced applications of proportional and drift chamber principles is embodied in the *time projection chamber* (TPC) illustrated schematically in Figure 4.14. This device consists of a cylindrical barrel, typically

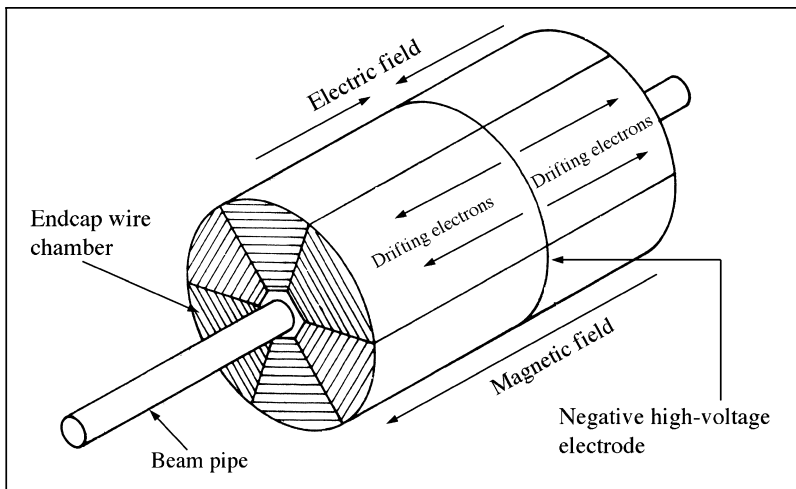


Figure 4.14 Schematic diagram of a time projection chamber (TPC) (adapted from Kl86, copyright Cambridge University Press)

¹²In the new generation of colliders, drift chambers are largely being replaced by detectors based on silicon.

2 m long and 1 m in diameter, surrounding the beam pipe of a collider. At each end of the chamber is a segmented layer of proportional counters. The electric drift field E , due to a negative high-voltage electrode plane at the centre of the chamber, and a strong magnetic field B are aligned parallel and anti-parallel to the axis of the cylinder. Because of this, the Lorentz forces on the drifting electrons vanish and electrons formed along the track of an ionizing particle emerging from the interaction point at the centre of the barrel, drift towards one of the endcaps along helical trajectories whose direction is parallel to the axis of the barrel. Their locations are measured by a set of anode wires located between rectangular cathodes in the endcaps. The remaining third coordinate necessary to reconstruct the position of a point on the track is found from the time it takes for the electrons to drift from the point of production to the endcaps where they are detected. The TPC has excellent spatial resolution.

Recently a more robust form of chamber has evolved, in which the wires are replaced by conductive metal strips on a printed circuit board. This is called a *microstrip gas chamber* (MSGC) and is being incorporated in experiments being designed for the new generation of accelerators currently planned or under construction.

Beyond the region of proportionality

Referring again to Figure 4.12, by increasing the external voltage still further one moves into a region where the output signal ceases to be proportional to the number of ion pairs produced and hence the incident energy. This is the region of *limited proportionality*. In this region a type of gas detector called a streamer tube operates, but this will not be discussed here. Eventually the process runs out of control and we enter the *Geiger–Müller region* where the output signal is independent of the energy lost by the incident particle. In this region a quenching agent is not used. Detectors working in this region are called Geiger–Müller counters. Physically they are similar to the simple cylindrical proportional counter and are widely used as portable radiation monitors in the context of safety regulations.

For completeness, we can mention that if the gas amplification factor is taken beyond the Geiger–Müller region, the avalanche develops moving plasmas or streamers. Recombination of ions then leads to visible light which can be made to generate an electrical output. Eventually complete breakdown occurs and a spark is emitted as the incident particle traverses the gas. Detectors in this region, called streamer and spark chambers (these were of parallel plate construction, rather than cylindrical), were widely used in the 1970s and 1980s and played an important role in hadron physics, but are no longer in general use.

4.4.2 Scintillation counters

For charged particles we have seen that energy losses occur due to excitation and ionization of atomic electrons in the medium of the detector. In suitable materials, called *scintillators*, a small fraction of the excitation energy re-emerges as visible light (or sometimes in the UV region) during de-excitation. In a scintillation counter this light passes down the scintillator and onto the face of a *photodetector* – a device that converts a weak photon signal to a detectable electric impulse. An important example of a photodetector is the *photomultiplier tube*, a schematic diagram of which is shown in Figure 4.15.

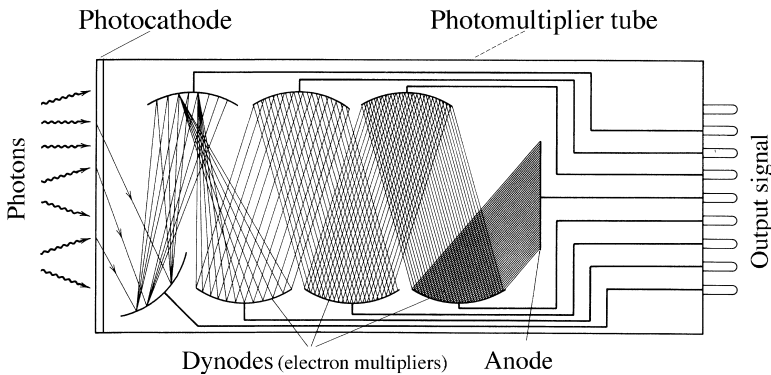


Figure 4.15 Schematic diagram of the main elements of a photomultiplier tube (adapted from Kr88, copyright John Wiley & Sons)

Electrons are emitted from the cathode of the photomultiplier by the photoelectric effect and strike a series of focusing dynodes. These amplify the electrons by secondary emission at each dynode and accelerate the particles to the next stage. The final signal is extracted from the anode at the end of the tube. The electronic pulse can be shorter than 10 ns if the scintillator has a short decay time. The scintillation counter is thus an ideal timing device and it is widely used for ‘triggering’ other detectors, i.e. its signal is used to decide whether or not to activate other parts of the detector, and whether to record information from the event. Commonly used scintillators are inorganic single crystals (e.g. caesium iodide) or organic liquids and plastics, and a modern complex detector in particle physics may use several tons of detector in combination with thousands of photomultiplier tubes.¹³ The robust and simple nature of the scintillation counter

¹³For example, the Super Kamiokande experiment mentioned in Chapter 3, which detected neutrino oscillations, although not using scintillation counters, has 13 000 photomultiplier tubes.

has made it a mainstay of experimental nuclear and particle physics since the earliest days of the subject.

Just as direct detection of neutrons is not possible by ionization methods, so the same is true using scintillators. However, the α -particle and the ${}^3\text{H}$ nucleus from the direct nuclear reaction ${}^6\text{Li}(n, \alpha){}^3\text{H}$ mentioned in Section 4.3.2 can produce light in a LiI crystal scintillator and forms the basis for detecting neutrons with energies up to about 20 MeV.

4.4.3 Semiconductor detectors

Solid-state detectors operate through the promotion of electrons from the valence band of a solid to the conduction band as a result of the entry of the incident particle into the solid. The resulting absence of an electron in the valence band (a ‘hole’) behaves like a positron. Semiconductor detectors are essentially solid-state ionization chambers with the electron–hole pairs playing the role of electron–ion pairs in gas detectors. In the presence of an electric field, the electrons and holes separate and collect at the electrodes, giving a signal proportional to the energy loss of the incident charged particle. Most semiconductor detectors use the principle of the junction diode. Since the band gap in some solids is as small as 1 eV and the energy loss required to produce a pair is only 3–4 eV on average (cf. the 30 eV required in a gas detector), a very large number of electron–hole pairs with only a small statistical fluctuation will be produced by a low-energy particle. Solid-state detectors are therefore very useful in detecting low-energy particles. Semiconductors (principally silicon or germanium) are used as a compromise between materials that have residual conductivity sufficient to enable conduction pulses due to single particles to be distinguished above background and those in which the charges carriers are not rapidly trapped in impurities in the material.

Such detectors have long been used in nuclear physics, where, for example, their excellent energy resolution and linearity, plus their small size and consequent fast response time, make them ideal detectors for γ -ray spectroscopy. Only recently have thin planar detectors become important in particle physics, because of the expense of covering large areas. Nevertheless, several square metres of semiconductor detector are being planned for experiments at the LHC.

One example of a solid-state detector is a *silicon microstrip detector*, where narrow strips of active detector are etched onto a thin slice of silicon, with gaps of the order of 10 μm , to give a tiny analogue of an MWPC. Arrays of such strips can then be used to form detectors with resolutions of the order of 5 μm . These are often placed close to the interaction vertex in a colliding beam experiment, with a view to studying events involving the decay of very short-lived particles. Another example is the *pixel detector*. A single-plane strip detector only gives position information in one dimension (orthogonal to the strip). A pixel detector improves on this by giving information in two dimensions from a single plane.

Solid-state ‘vertex detectors’ are becoming increasingly important in particle physics and have been incorporated in several of the multi-component detectors designed for use in the new generation of colliders. Their main advantage is their superb spatial resolution; a disadvantage is their limited ability to withstand radiation damage.

4.4.4 Particle identification

Methods of identifying particles are usually based on determining the mass of the particle by a simultaneous measurement of its momentum together with some other quantity. At low values of $\gamma = E/mc^2$, measurements of the rate of energy loss dE/dx can be used, while muons may be characterized by their unique penetrating power in matter, as we have already seen. Here we concentrate on methods based on measuring the velocity or energy, assuming always that the momentum is known. We thus need to start with explaining how momenta are measured.

Measurement of momentum

The momentum of a charged particle is usually determined from the curvature of its track in an applied magnetic field. It is common practice to enclose track chambers in a magnetic field to perform momentum analysis. An apparatus that is dedicated to measuring momentum is called a *spectrometer*. It consists of a magnet and a series of detectors to track the passage of the particles. The precise design depends on the nature of the experiment being undertaken. For example, in a fixed-target experiment at high energies, the reaction products are usually concentrated in a narrow cone around the initial beam direction, whereas in colliding-beam experiments spectrometers must completely surround the interaction region to obtain full angular coverage.

Magnet designs vary. Dipole magnets typically have their field perpendicular to the beam direction. They have their best momentum resolution for particles emitted forward and backward with respect to the beam direction, and are often used in fixed-target experiments at high energies. However, the beam will be deflected, and so at colliders this must be compensated for elsewhere to keep the particles in orbit. Compensating magnets are present in the ‘layered detectors’ shown in Section 4.6 below. At colliders, the most usual magnet shape is the solenoid, where the field lines are essentially parallel to the beam direction. This device is used in conjunction with cylindrical tracking detectors, like jet chambers, and has its best momentum resolution for particles perpendicular to the beam direction.

We now turn to methods of measuring velocity.

Time-of-flight

The simplest method, in principle, is to measure the time of flight between, for example, two scintillation counters. If the distance between them is L , the time difference for two particles of masses m_1 and m_2 travelling with velocities v_1 and v_2 , is

$$\Delta t = t_2 - t_1 = \frac{L}{c} \left(\frac{1}{\beta_1} - \frac{1}{\beta_2} \right), \quad (4.25)$$

where $\beta \equiv v/c$. For a common momentum p , Equation (4.25) may be written, using¹⁴ $E = pc/\beta$,

$$\Delta t = \frac{L}{pc^2} \left[(m_2^2 c^4 + p^2 c^2)^{1/2} - (m_1^2 c^4 + p^2 c^2)^{1/2} \right]. \quad (4.26)$$

We are interested in the situation where $m_2 \approx m_1 \equiv m$ and $v_2 \approx v_1 \equiv v$. In this case, setting $\Delta m \equiv m_2 - m_1$, the non-relativistic limit of Equation (4.26) is $\Delta t = t \Delta m/m$ and using $v = L/t$, we have

$$\frac{\Delta m}{m} = \Delta t \frac{\beta c}{L}. \quad (4.27)$$

Thus, for example, taking typical values of $\beta = 0.2$, $L = 100 \text{ cm}$ and $\Delta t = 2 \times 10^{-10} \text{ s}$ (assuming the timing is done using a scintillation counter), $\Delta m/m$ can be determined to about 1 per cent for low-energy particles. This method is used, for example, in nuclear physics experiments using very low-energy neutron beams.

However, since all high-energy particles have velocities close to the speed of light, the method ceases to be useful for even quite moderate momenta. This can be seen by taking the relativistic limit of Equation (4.26), when we have

$$\Delta t \approx \frac{Lc}{2p^2} (m_2^2 - m_1^2), \quad (4.28)$$

which for $m_2 \approx m_1 \equiv m$, $v_2 \approx v_1 \equiv c$, and using $p = \gamma mc$ becomes

$$\frac{\Delta m}{m} = \frac{\gamma^2 c \Delta t}{L}. \quad (4.29)$$

For example, using our previous values for L and Δt , Equation (4.29) shows that the method is not useful for values of γ above about three, which corresponds to a momentum of only about 3 GeV/c for nucleons. Of course this could be extended by taking longer flight paths, but only at greater expense in instrumentation.

¹⁴See Appendix B.

Čerenkov counters

The most important identification method for high-energy particles is based on the Čerenkov effect. When a charged particle with velocity v traverses a dispersive medium of refractive index n , excited atoms in the vicinity of the particle become polarized, and if v is greater than the speed of light in the medium c/n , a part of the excitation energy reappears as coherent radiation emitted at a characteristic angle θ to the direction of motion. The necessary condition $v > c/n$ implies $\beta n > 1$ and by considering how the waveform is produced¹⁵ it can be shown that $\cos \theta = 1/\beta n$ for the angle θ , where $\beta = v/c$ as usual. A determination of θ is thus a direct measurement of the velocity.¹⁶

Čerenkov radiation appears as a continuous spectrum and may be collected onto a photosensitive detector. Its main limitation from the point of view of particle detection is that very few photons are produced. The number of photons $N(\lambda)d\lambda$ radiated per unit path length in a wavelength interval $d\lambda$ can be shown to be

$$N(\lambda)d\lambda = 2\pi\alpha \left(1 - \frac{1}{\beta^2 n^2}\right) \frac{d\lambda}{\lambda^2} < 2\pi\alpha \left(1 - \frac{1}{n^2}\right) \frac{d\lambda}{\lambda^2} \quad (4.30)$$

and so vanishes rapidly as the refractive index approaches unity. The maximum value occurs for $\beta = 1$, which for a particle with unit charge, corresponds to about 200 photons/cm in the visible region in water and glass. These numbers should be compared with the 10^4 photons/cm emitted by a typical scintillator. Because the yield is so small, appreciable lengths are needed to give enough photons, and gas Čerenkov counters in particular can be several metres long.

Čerenkov counters are used in two different modes. The first is as a *threshold counter* to detect the presence of particles whose velocities exceed some minimum value. Suppose that two particles with β values β_1 and β_2 at some given momentum p are to be distinguished. If a medium can be found such that $\beta_1 n > 1 \geq \beta_2 n$, then particle 1 will produce Čerenkov radiation but particle 2 will not. Clearly, to distinguish between highly relativistic particles with $\gamma \gg 1$ also requires $n \approx 1$, so that from Equation (4.30) very few photons are produced. Nevertheless, common charged particles can be distinguished in this way up to at least 30 GeV/c.

Another device is the so-called *ring-image* Čerenkov detector which is a very important device in both fixed-target machines and colliders. If we assume that the particles are not all travelling parallel to a fixed axis, then the radiating medium can be contained within two concentric spherical surfaces of radii R and $2R$ centred on the target or interaction region where the particles are produced, as illustrated in Figure 4.16. The outer surface is lined with a mirror, which focuses

¹⁵This is Huygens' construction in optics.

¹⁶For the discovery and interpretation of this effect, Pavel Čerenkov, Ilya Frank and Igor Tamm were awarded the 1958 Nobel Prize in Physics.

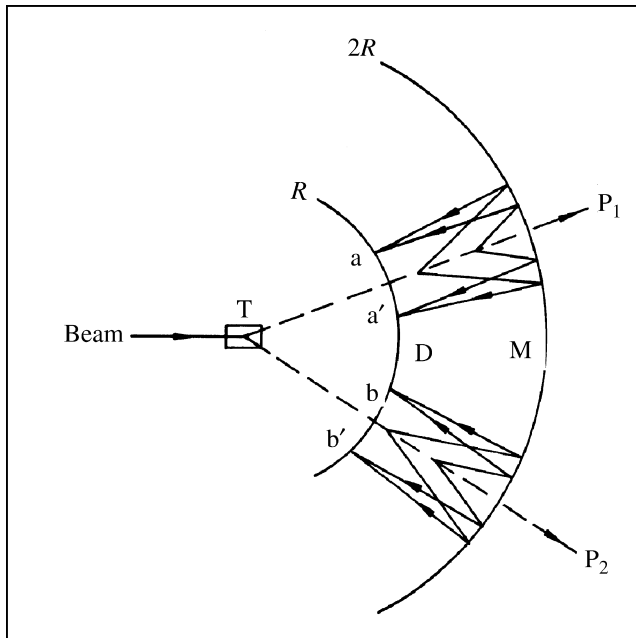


Figure 4.16 Two particles P_1 and P_2 , produced from the target T, emit Čerenkov radiation on traversing a medium contained between two spheres of radius R and $2R$. The mirror M on the outer sphere focuses the radiation into ring images at aa' and bb' on the inner detector sphere D. The radii of the ring images depend on the angle of emission of the Čerenkov radiation and hence on the velocities of the particles

the Čerenkov radiation into a ring at the inner detector surface. The radius of this ring depends on the angle θ at which the Čerenkov radiation is emitted, and hence on the particle velocity v . It is determined by constructing an image of the ring electronically. This was the technique used in the Super Kamiokande detector discussed in Chapter 3 to detect relativistic electrons and muons produced by neutrino interactions. In that experiment the radiating medium was pure water.

4.4.5 Calorimeters

Calorimeters are an important class of detector used for measuring the energy and position of a particle by its total absorption and are widely used. They differ from most other detectors in that (1) the nature of the particle is changed by the detector, and (2) they can detect neutral as well as charged particles. A calorimeter may be a homogeneous absorber/detector to detect photons and electrons. In early devices this was often a block of lead glass, but is now more likely to be scintillator such as CsI. Alternatively, it can be a sandwich construction with separate layers of absorber (e.g. a metal such as lead) and detector (scintillator, MWPC etc.). The latter are also

known as ‘sampling calorimeters’. During the absorption process, the particle will interact with the material of the absorber, generating secondary particles which will themselves generate further particles and so on, so that a cascade or shower, develops. For this reason calorimeters are also called ‘shower counters’.

The shower is predominantly in the longitudinal direction due to momentum conservation, but will be subject to some transverse spreading due both to multiple Coulomb scattering and the transverse momentum of the produced particles. Eventually all, or almost all, of the primary energy is deposited in the calorimeter, and gives a signal in the detector part of the device.

There are several reasons why calorimeters are important, especially at high energies:

- they can detect neutral particles, by detecting the charged secondaries;
- the absorption process is statistical (and governed by the Poisson distribution), so that the relative precision of energy measurements $\Delta E/E$ varies as $E^{-\frac{1}{2}}$ for large E , which is a great improvement on high-energy spectrometers where $\Delta E/E$ varies as E^2 ;
- the signal produced can be very fast, of the order of (10–100) ns, and is ideal for making triggering decisions.

Although it is possible to build calorimeters that preferentially detect just one class of particle (electrons and photons, or hadrons) it is also possible to design detectors that serve both purposes. Since the characteristics of electromagnetic and hadronic showers are somewhat different it is convenient to describe each separately. In practice, it is common to have both types in one experiment with the hadron calorimeter stacked behind the electromagnetic one.

Electromagnetic showers

When a high-energy electron or positron interacts with matter we have seen that the dominant energy loss is due to bremsstrahlung, and for the photons produced the dominant absorption process is pair production. Thus the initial electron will, via these two processes, lead to a cascade of e^\pm pairs and photons, and this will continue until the energies of the secondary electrons fall below the critical energy E_C where ionization losses equal those from bremsstrahlung. This energy is roughly given by $E_C \approx 600 \text{ MeV}/Z$.

Most of the correct qualitative features of shower development may be obtained from the following very simple model. We assume:

- each electron with $E > E_C$ travels one radiation length and then gives up half of its energy to a bremsstrahlung photon;

- each photon with $E > E_C$ travels one radiation length and then creates an electron–positron pair with each particle having half the energy of the photon;
- electrons with $E < E_C$ cease to radiate and lose the rest of their energy by collisions;
- ionization losses are negligible for $E > E_C$.

A schematic diagram of the approximate development of a shower in an electromagnetic calorimeter assuming this simple model is shown in Figure 4.17.

If the initial electron has energy $E_0 \gg E_C$, then after t radiation lengths the shower will contain 2^t particles, which consist of approximately equal numbers of electrons, positrons and photons each with an average energy

$$E(t) = E_0/2^t. \tag{4.31}$$

The multiplication process will cease abruptly when $E(t) = E_C$, i.e. at $t = t_{\max}$ where

$$t_{\max} = t(E_C) \equiv \frac{\ln(E_0/E_C)}{\ln 2} \tag{4.32}$$

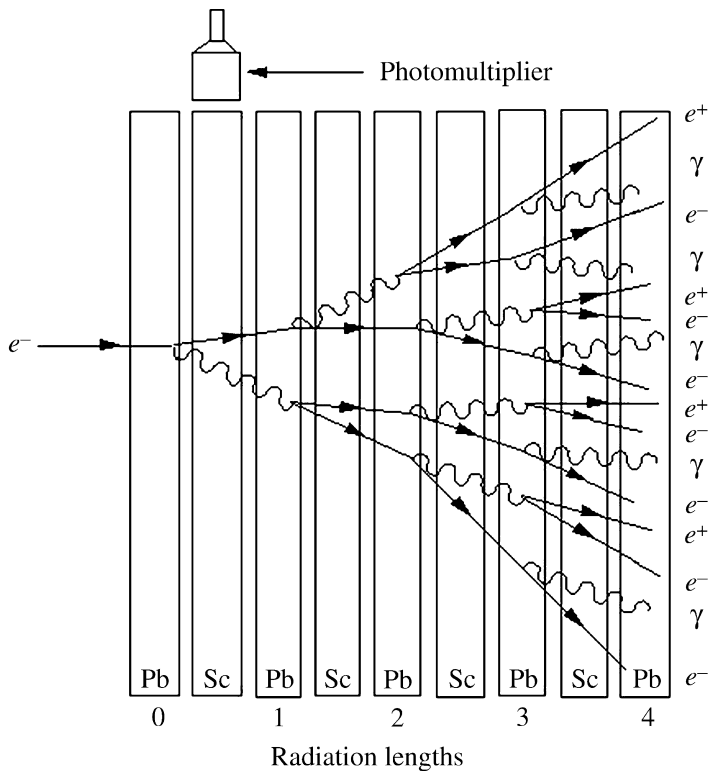


Figure 4.17 Approximate development of an electromagnetic shower in a sampling calorimeter assuming the simple model described in the text; the calorimeter consists of alternate layers of lead (Pb) and a scintillator (Sc), the latter attached to photomultipliers (one only shown)

and the number of particles at this point will be

$$N_{\max} = \exp[t_{\max} \ln 2] = E_0/E_C. \quad (4.33)$$

The main features of this simple model are observed experimentally, and in particular the maximum shower depth increases only logarithmically with primary energy. Because of this, the physical sizes of calorimeters need increase only slowly with the maximum energies of the particles to be detected. The energy resolution of a calorimeter, however, depends on statistical fluctuations, which are neglected in this simple model, but for an electromagnetic calorimeter it is typically $\Delta E/E \approx 0.05/E^{1/2}$, where E is measured in GeV.

Hadronic showers

Although hadronic showers are qualitatively similar to electromagnetic ones, shower development is far more complex because many different processes contribute to the inelastic production of secondary hadrons. The scale of the shower is determined by the nuclear absorption length defined earlier. Since this absorption length is larger than the radiation length, which controls the scale of electromagnetic showers, hadron calorimeters are thicker devices than electromagnetic ones. Another difference is that some of the contributions to the total absorption may not give rise to an observable signal in the detector. Examples are nuclear excitation and leakage of secondary muons and neutrinos from the calorimeter. The loss of ‘visible’ or measured energy for hadrons is typically 20–30 per cent greater than for electrons.

The energy resolution of calorimeters is in general much worse for hadrons than for electrons and photons because of the greater fluctuations in the development of the hadron shower. Depending on the proportion of π^0 s produced in the early stages of the cascade, the shower may develop predominantly as an electromagnetic one because of the decay $\pi^0 \rightarrow \gamma\gamma$. These various features lead to an energy resolution typically a factor of 5–10 poorer than in electromagnetic calorimeters.

4.5 Layered Detectors

As stated earlier, in particle physics it is necessary to combine several detectors in a single experiment to extract the maximum amount of information from it. Typically, working out from the interaction region, there will be a series of wire chambers, followed further out by calorimeters and at the outermost limits, detectors for muons, the most penetrating particles to be detected. The whole device is usually in a strong magnetic field so that momentum measurements may be made. We will illustrate the general features by three examples.

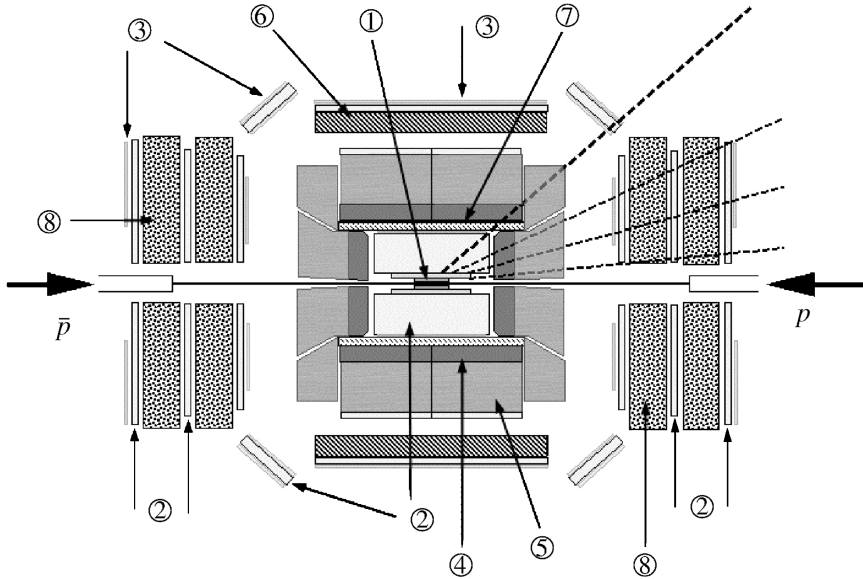


Figure 4.18 The CDF detector at the $p\bar{p}$ collider at Fermilab, USA (Fermilab Graphic, reproduced with permission)

The first is the $p\bar{p}$ Collider Detector at Fermilab (CDF), which is shown schematically in Figure 4.18. The detection of the top quark and the measurement of its mass were first made using this device. The dashed lines indicate some particles produced in the collision. CDF is a large device, being approximately 8 m wide and 26 m in overall length. The beams of protons and antiprotons enter from each end through focusing quadrupole magnets and interact in the central intersection region where there is a silicon vertex detector (1) to detect very short-lived particles. The intersection point is surrounded by a 2000 tonne detector system which, in addition to the vertex detector, consists of inner drift chambers (2), electromagnetic calorimeters (4), hadron calorimeters (5) time-of-flight detectors (not indicated) and further drift chambers (2) on the outside to detect muons. The whole system is in a magnetic field with the solenoid coil shown at (7) and steel shielding at (6). The rest of the detector consists of two symmetrical sets of drift chambers (2) sandwiched between scintillation counters (3) and magnetic toroids (8) to provide momentum measurements, primarily for muons.

The second example, shown schematically in Figure 4.19, is the ATLAS detector currently under construction for use at the Large Hadron Collider (LHC). It is hoped that this and other detectors at the LHC will be able to detect the important Higgs boson, if it exists, and so help solve one of the outstanding current problems in particle physics – the origin of mass. The ATLAS detector is even larger than the CDF detector and measures about 22 m high and 44 m long, with an overall weight of approximately 7000 tonnes.

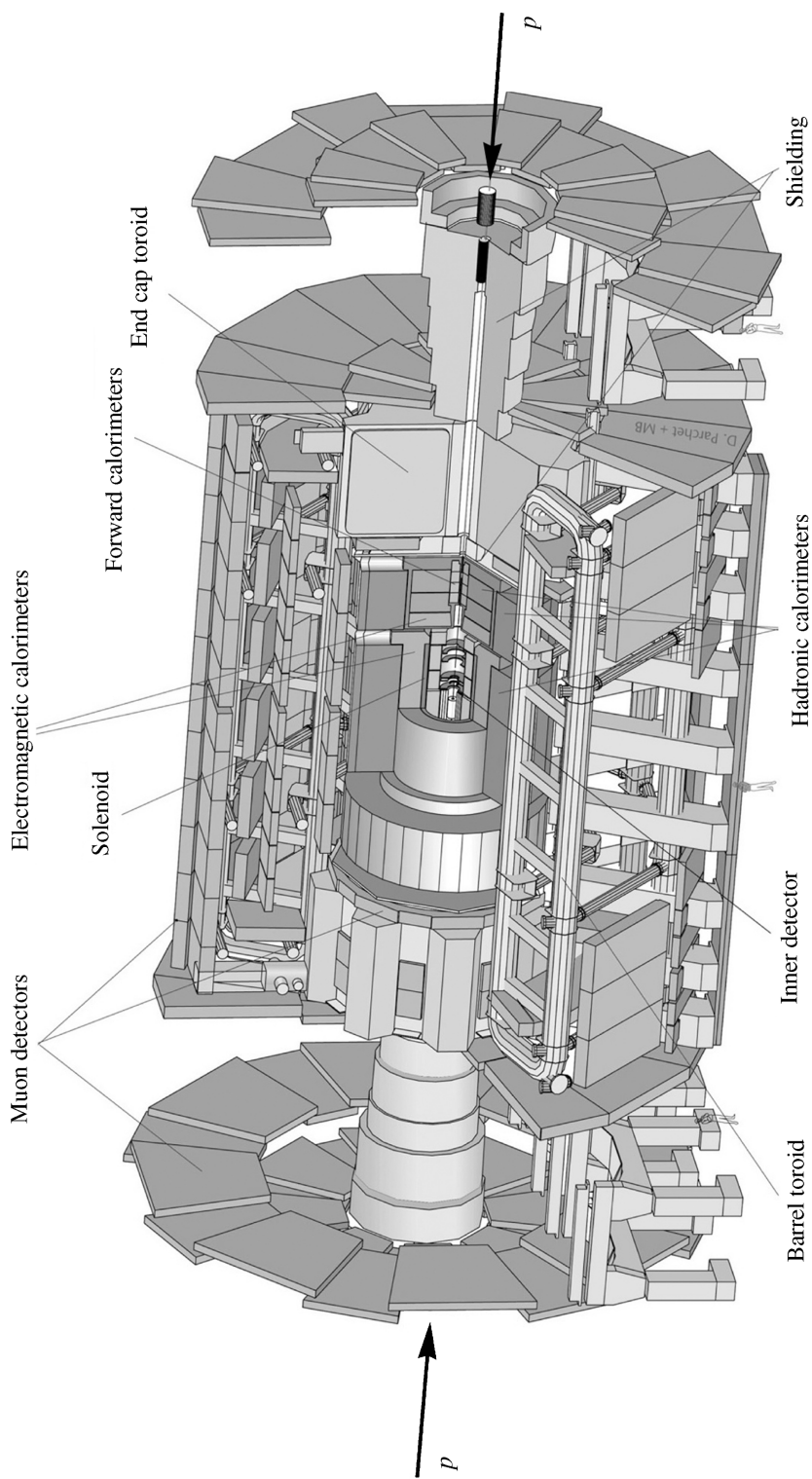


Figure 4.19 The ATLAS detector under construction for use at the pp collider LHC (also under construction) at CERN, Geneva, Switzerland (CERN photo, reproduced with permission)

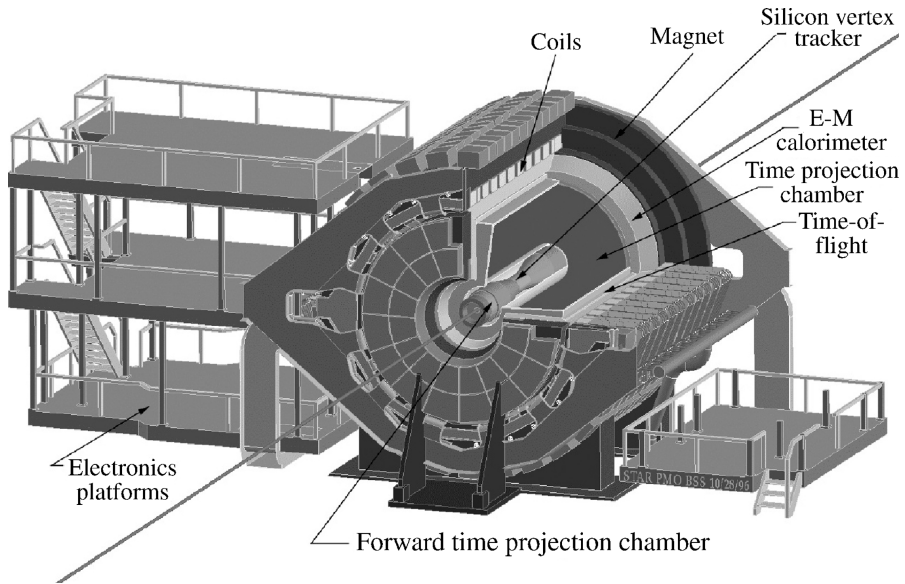


Figure 4.20 The STAR detector at the RHIC accelerator at Brookhaven National Laboratory, USA. (Courtesy of Brookhaven National Laboratory)

Finally, Figure 4.20 shows the STAR detector at the RHIC accelerator at Brookhaven National Laboratory. This detects events resulting from the collisions of heavy ions, typically those of fully-stripped gold nuclei, where the final state may contain many thousands of particles. An example of an event is shown in Figure 9.12.

Problems

- 4.1 At a collider, a 20 GeV electron beam collides with a 300 GeV proton beam at a crossing angle of 10° . Evaluate the total centre-of-mass energy and calculate what beam energy would be required in a fixed-target electron machine to achieve the same total centre-of-mass energy.
- 4.2 What is the length L of the longest drift tube in a linac which operating at a frequency of $f = 20$ MHz is capable of accelerating ^{12}C ions to a maximum energy of $E = 100$ MeV?
- 4.3 Alpha particles are accelerated in a cyclotron operating with a magnetic field of magnitude $B = 0.8$ T. If the extracted beam has an energy of 12 MeV, calculate the extraction radius and the orbital frequency of the beam (the so-called *cyclotron frequency*).

- 4.4 Protons with momentum 50 GeV/c are deflected through a collimator slit 2 mm wide by a bending magnet 1.5 m long which produces a field of 1.2 T. How far from the magnet should the slit be placed so that it accepts particles with momenta in the range 49–51 GeV/c?
- 4.5 Estimate the minimum length of a gas Čerenkov counter that could be used in threshold mode to distinguish between charged pions and charged kaons with momentum 20 GeV/c. Assume that a minimum of 200 photons need to be radiated to ensure a high probability of detection. Assume also that the radiation covers the whole visible spectrum between 400 nm and 700 nm and neglect the variation with wavelength of the refractive index of the gas.
- 4.6 An e^+e^- collider has a diameter of 8 km and produces beams of energy 45 GeV. Each beam consists of 12 bunches each containing 3×10^{11} particles. The bunches have a cross-sectional area of 0.02 mm². What is the luminosity of the machine in units of cm⁻²s⁻¹?
- 4.7 What are the experimental signatures and with what detectors would one measure: (a) the decay $Z \rightarrow b\bar{b}$, and (b) $W \rightarrow e\nu$ and $W \rightarrow \mu\nu$.
- 4.8 The reaction $e^+e^- \rightarrow \tau^+\tau^-$ is studied using a collider with equal beam energies of 5 GeV. The differential cross-section is given by

$$\frac{d\sigma}{d\Omega} = \frac{\alpha^2 \hbar^2 c^2}{4E_{\text{cm}}^2} (1 + \cos^2 \theta)$$

where E_{cm} is the total centre-of-mass energy and θ is the angle between the incoming e^- and the outgoing τ^- . If the detector can only record an event if the $\tau^+\tau^-$ pair makes an angle of at least 30° relative to the beam line, what fraction of events will be recorded? What is the total cross-section for this reaction in nanobarns? If the reaction is recorded for 10⁷s at a luminosity of $L = 10^{31}$ cm⁻²s⁻¹, how many events are expected?

Suppose the detector is of cylindrical construction and at increasing radii from the beam line there is a drift chamber, an electromagnetic calorimeter, a hadronic calorimeter and finally muon chambers. If in a particular event the τ^- decays via $\tau^- \rightarrow \mu^- + \bar{\nu}_\mu + \nu_\tau$ and the τ^+ decays to $\tau^+ \rightarrow e^+ + \bar{\nu}_\tau + \nu_e$, what signals would be observed in the various parts of the detector?

- 4.9 A charged particle with speed v moves in a medium of refractive index n . By considering the wavefronts emitted at two different times, derive a relation for the angle θ of the emitted Čerenkov radiation relative to the particle's direction in terms of $\beta = v/c$ and n . What is the maximum angle of emission and to what limit does it correspond?

If the momentum p of the particle is known from other detectors, show that the mass squared x of the particle is given by $x = (mc^2)^2 = p^2 c^2 (n^2 \cos^2 \theta - 1)$. If the error on the momentum is negligible, show, by taking derivatives of this expression, that for very relativistic particles, the standard error σ_x on x is approximately

$$\sigma_x \approx 2p^2 c^2 \sqrt{(n^2 - 1)} \sigma_\theta,$$

where σ_θ is the standard error on θ .

- 4.10** Estimate the thickness of iron through which a beam of neutrinos with energy 300 GeV must travel if 1 in 10^9 of them is to interact. Assume that at high energies the neutrino-nucleon total cross-section is given approximately by $\sigma_\nu \approx 10^{-38} E_\nu \text{ cm}^2$ where E_ν is given in GeV. The density of iron is $\rho = 7.9 \text{ g cm}^{-3}$.
- 4.11** An electron with an initial energy of 2 GeV traverses 10 cm of water with a radiation length of 36.1 cm. Calculate its final energy. How would the energy loss change if the particle were a muon rather than an electron?
- 4.12** A beam of neutrons with kinetic energy 0.1 eV and intensity 10^6 s^{-1} is incident normally on a thin foil of $^{235}_{92}\text{U}$ of effective thickness $10^{-1} \text{ kg m}^{-2}$. The beam can undergo (1) isotropic elastic scattering, with a cross section $\sigma_{\text{el}} = 3 \times 10^{-2} \text{ b}$, (2) radiative capture, with a cross-section $\sigma_{\text{cap}} = 10^2 \text{ b}$, or (3) it can fission a $^{235}_{92}\text{U}$ nucleus, with a cross-section $\sigma_{\text{f}} = 3 \times 10^2 \text{ b}$. Calculate the attenuation of the beam and the flux of elastically-scattered particles 5 m from the foil.
- 4.13** A positron with laboratory energy 50 GeV interacts with the atomic electrons in a lead target to produce $\mu^+\mu^-$ pairs. If the cross-section for this process is given by $\sigma = 4\pi\alpha^2\hbar^2c^2/3(E_{\text{CM}})^2$, calculate the positron's interaction length. The density of lead is $\rho = 1.14 \times 10^7 \text{ kg m}^{-3}$.
- 4.14** A liquid hydrogen target of volume 125 cm^3 and density 0.071 g cm^{-3} is bombarded with a mono-energetic beam of negative pions with a flux $2 \times 10^7 \text{ m}^{-2} \text{ s}^{-1}$ and the reaction $\pi^- + p \rightarrow \pi^0 + n$ observed by detecting the photons from the decay of the π^0 . Calculate the number of photons emitted from the target per second if the cross-section is 40 mb.
- 4.15** Assuming the Bethe–Bloch formula is valid for low energies, show that the rate of ionization has a maximum (the Bragg peak) and find the kinetic energy of protons in iron for which this maximum would occur.
- 4.16** A cylindrical proportional chamber has a central anode wire of radius 0.02 mm and an outer cathode of radius 10 mm with a voltage of 500 V applied between them. What is the electric field at the surface of the anode? If the threshold for ionization by collision is 750 kV m^{-1} and the mean free path of the particles being detected is $4 \times 10^{-6} \text{ m}$, estimate the number of ion pairs produced per primary particle.